

31

Future directions

We have seen several examples of existing experimental results from TJNAF (CEBAF), and have discussed their implications for nuclear and particle physics. In the author's opinion, the best way to get a feel for the quality and impact of the future CEBAF physics program is to show anticipated error bars, kinematic range, and event modeling in a few selected examples. While reluctant to show anticipated data because so much work lies ahead in actually carrying out the experiments, such a significant effort has already gone into modeling the detectors, magnetics, acceptances, efficiencies, electronics, and event rates for the real experiments that the author feels justified in presenting this material; it is taken from the proposals.¹ The experimental program is dynamic and constantly evolving. Where data now exist, they more than satisfy the expectations. The following discussion only represents one snapshot in time. It is based on talks the author gave on the CEBAF scientific program, when the experimental program was still one of anticipation [Wa93, Wa94].

As one example, Fig. 31.1 shows the anticipated errors on the charge form factor of the proton G_{Ep} (relative to the dipole fit) from the polarization transfer measurement $^1\text{H}(\vec{\epsilon}, e \vec{p})$ at CEBAF as anticipated in PR 89-014 [Pe89]. This polarization transfer experiment measures the product of the magnetic and electric form factors of the proton [Ar81]. Since the magnetic form factor is well known, this interference term allows an accurate determination of G_{Ep} . To get a feel for the validity of such projections, Fig. 29.6 shows subsequent actual data on the measurement of G_{Ep}/G_{Mp} at TJNAF [Jo00]. The data are indeed superb.

Figure 31.2 shows the anticipated error bars on the determination of G_{En} from two experiments: a polarization transfer measurement $^2\text{H}(\vec{\epsilon}, e' \vec{n})$ in CEBAF PR 89-005 [Ma89a] similar to that discussed above; and a

¹ The proposals are available in the library at TJNAF.

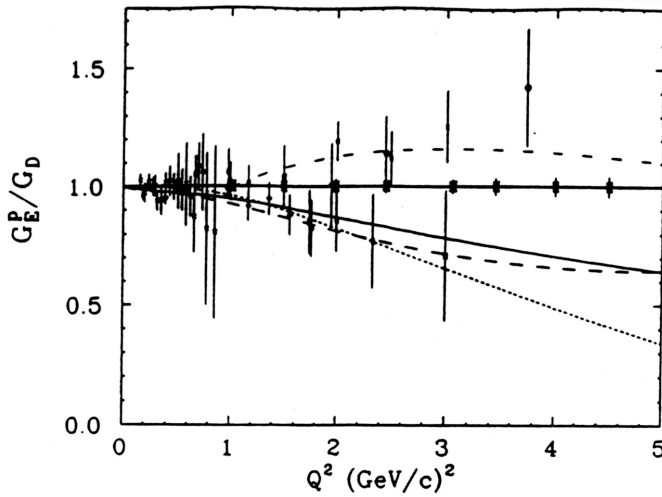


Fig. 31.1. Projected error bars in G_{Ep} in polarization transfer measurement ${}^1\text{H}(\vec{e}, e\vec{p})$ at CEBAF. From PR 89-014 [Pe89, Wa93]. Here $k \equiv Q$.

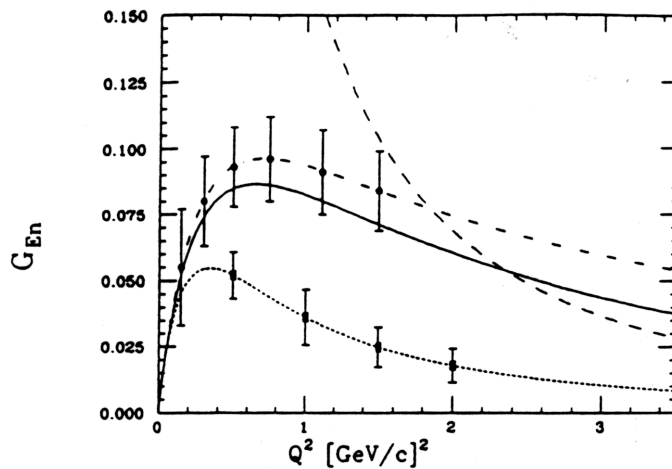


Fig. 31.2. Projected error bars on G_{En} from polarization transfer measurement ${}^2_1\text{H}(\vec{e}, e' \vec{n})$ in CEBAF PR 89-005 (upper); and polarized target experiment ${}^2_1\vec{\text{H}}(\vec{e}, e' n)$ in CEBAF PR 89-018 [Ma89a, Da89, Wa93]. Here $k \equiv Q$.

coincidence measurement with a polarized target ${}^2_1\vec{\text{H}}(\vec{e}, e' n)$ in CEBAF PR 89-018 which also determines G_{En} through an interference term [Da89].² Since the measurement of G_{En} ultimately involves nuclear physics (there are as yet no free neutron targets), it is important to have complementary

² The error bars are relative to the different theoretical estimates.

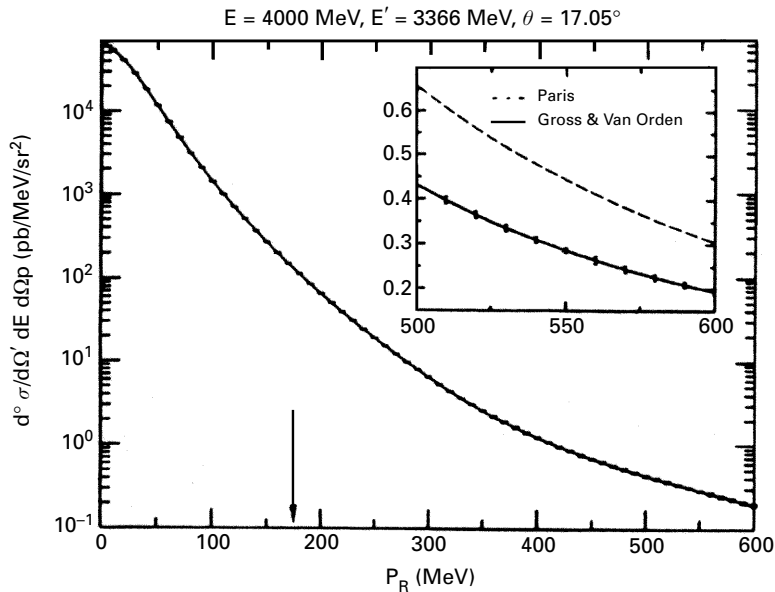


Fig. 31.3. Projected range and error bars in ${}^2\text{H}(e, e' p)$ from CEBAF PR 89-028 [Fi89, Wa93].

determinations. Both of the charge distributions G_{En} and G_{Ep} directly reflect the internal structure of the baryon; the theoretical description of the accurate measurements of these charge distributions will continue to provide a benchmark challenge to quark models and QCD.

Consider next the nuclear coincidence reaction ${}^2\text{H}(\bar{e}, e' \bar{p})$ to be measured in CEBAF PR 89-028 [Fi89]. This polarization transfer experiment explores the spin structure of the deuteron in unrivaled detail; it also provides an important calibration for the measurement of G_{En} by a similar procedure. In the course of this experiment, the momentum distribution in the deuteron will be determined at the same kinematics. Plotted in Fig. 31.3 are the anticipated range and error bars in the determination of the basic nuclear coincidence cross section ${}^2\text{H}(e, e' p)$ to be measured in PR 89-028 [Fi89]. The arrow indicates the extent of existing data, and the inset demonstrates that the experiment will distinguish between different models; one calculation shown uses a good two-nucleon potential, the other a relativistic boson-exchange description.³ Elastic charge scattering essentially measures the Fourier transform of the spatial density (square of the wave function); the $(e, e' p)$ reaction essentially measures the Fourier transform of the wave function (whose square is the momentum density)

³ The calculation is for illustration; it assumes plane waves in the final state and neglects exchange currents.

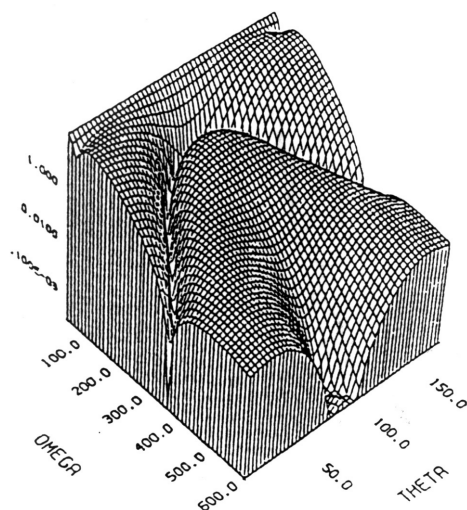


Fig. 31.4. Model calculation of in-plane Coulomb response surface for the reaction ${}^{18}_{10}\text{Ne}(e, e' 2p){}^{16}_8\text{O}(\text{g.s.})$ at $(\varepsilon_1, \theta_e) = (1 \text{ GeV}, 20^\circ)$; see text [Da92, Wa93].

—these are complementary quantities, and by measuring both one can examine the structure of this fundamental two-nucleon bound state in unprecedented detail.

Consider the results of a very simple model calculation, meant only to provide some guidance for explorations into new territory. In principle, the most direct way to examine short-range correlations is to study two-nucleon emission with extreme kinematics. Figure 31.4 shows a preliminary analysis by John Dawson of the in-plane Coulomb response for the triple coincidence ${}^{18}_{10}\text{Ne}(e, e' 2p){}^{16}_8\text{O}(\text{g.s.})$ [Da92] — this reaction is forbidden in a single-particle model. Here the initial wave function is the correlated relative ${}^1\text{S}_0$ state obtained by solving the Bethe–Goldstone equation with a two-nucleon potential for the interacting $(\pi 1d_{5/2})^2$ pair in the presence of the ${}^{16}_8\text{O}$ core.⁴ The total energy and C-M momentum of the pair are $(\omega, \mathbf{P} = \mathbf{p}_1 + \mathbf{p}_2 = \boldsymbol{\kappa})$ and θ is the angle between the relative momentum of the pair $2\mathbf{p} = \mathbf{p}_1 - \mathbf{p}_2$ and $\boldsymbol{\kappa}$. Plane wave final states are used in this initial calculation. Note the characteristic diffraction minimum as ω is increased and characteristic angular distribution of the 2-proton final state. In the present approximation, this surface measures the sum of the Fourier transforms of the two-nucleon correlation function with respect to $\mathbf{p} \pm \boldsymbol{\kappa}/2$. This calculation was motivated by a presentation of William Hersman at PAC5 (Fifth Program Advisory Committee Meeting) at CEBAF, in which he showed a similar model surface for the basic nuclear two-proton

⁴ This calculation and wave function are given in [Fe71].

coincidence experiment ${}^3\text{He}(e, e'2p)$ that will be studied in CEBAF PR 89-031 [He89]. This experiment will map out the two-proton wave function in this three-nucleon system — an unprecedented measurement, fundamental to our understanding of nuclear physics.⁵

Consider next pion production and the internal dynamics of the nucleon. In CEBAF PR 89-037 [Bu89], precision angular distributions will be measured on the first nucleon resonance at $W = 1232$ MeV with varying k^2 for the reactions ${}^1\text{H}(e, e' p)\pi^0$, ${}^1\text{H}(e, e' \pi^+)n$, and ${}^2\text{H}(e, e' \pi^-)pp$. The contributing multipoles can then be extracted from these angular correlation measurements. The resonant target transition is $(1/2^+, 1/2) \rightarrow (3/2^+, 3/2)$.

As discussed previously, the electric quadrupole transition E_{1+} is particularly interesting. Quark bag models of the nucleon, with a one-gluon exchange interaction, indicate that the bag may deform — similar to the deformation of the deuteron arising from the tensor force. As with even-even deformed nuclei, the nucleon can have no quadrupole moment in its ground state, so the most direct evidence for this deformation would show up in this transition amplitude. In the quark model, the above transition to the $P_{33}(1232)$ is predominantly spin-flip magnetic dipole M_{1+} . The E_{1+} is, in fact, observed to be small, and it is only very poorly known; this is illustrated in Fig. 28.2, which shows the existing world's data on $\text{Re}(E_{1+}^* M_{1+})/|M_{1+}|^2$ at the $\Delta(1232)$ at the time of CEBAF PR 89-037 [Bu89]; Fig. 28.3 shows the projected range and error bars in that proposal. Note, in particular, the expansion of the vertical scale in this second figure. The subsequent actual experimental results for this quantity have been shown previously in Fig. 28.4, more than meeting expectations.

At CEBAF, the internal dynamics of the nucleon will be studied with unrivaled precision. These measurements will provide deep insight into the dynamical consequences of QCD. The accurate new data will continue to provide benchmark tests for theoretical quark-model and QCD descriptions of the nucleon — the basic building block of matter.

A simulation of the CLAS detector output for observation of meson production through the reaction ${}^1\text{H}(\gamma, p)X$ is shown in Fig. 31.5 from PR 91-008 [Ri91]. Here the tagging of the photon and the measurement of the proton determine the missing mass of X, and well-defined peaks are seen for the two-body reactions producing $(\pi^0, \eta, \omega, \eta')$ at $E_\gamma = 1.7$ GeV. The π^0 production has already been referred to. The production of η with isospin $T = 0$ provides a selective mechanism to study the $T = 1/2$ nucleon resonances. CEBAF PR 89-039 [Dy89] utilizes the fact that the $S_{11}(1535)$ resonance has a large branching ratio into the η channel to selectively study the behavior of this state with high precision out to large k^2 . This

⁵ More detailed calculations of the process $(e, e' 2N)$ on nuclei are described in [Ry96, Ry97, Ry00].

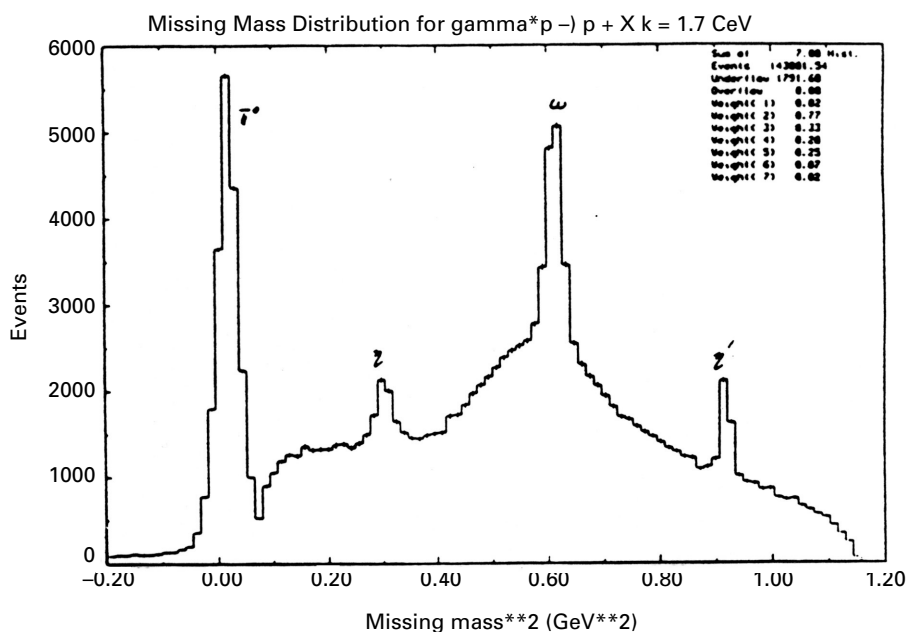


Fig. 31.5. CLAS simulation of missing-mass determination of meson production through the reaction ${}^1\text{H}(\gamma, p)\text{X}$ at $E_\gamma = 1.7\text{GeV}$. The abscissa is in GeV^2 . From CEBAF PR 91-008 [Ri91, Wa93].

state is particularly interesting because its inelastic form factor appears to fall anomalously slowly. Both η production, and the production of the $T = 0$ ω meson studied in PR 91-024 [Fu91], can be used to selectively search for nucleon resonances that couple only very weakly to pions. The η and η' signals also provide the opportunity to study the structure of these mesons themselves in PR 91-008 [Ri91].

An important feature of coincident electron scattering is that the baryon levels in the $S = -1$ sector can *also* be accessed with the $(e, e' K^+)$ reaction. In fact, PR 89-024 will look at the resulting photon transitions between the low-lying levels in this sector — a lovely extension of traditional nuclear γ spectroscopy [Mu89]. A CLAS simulation of the reaction ${}^1\text{H}(\gamma, K^+)\Lambda$ and subsequent decay $\Lambda \rightarrow p + \pi^-$ from PR 89-004 is shown in Fig. 31.6 [Sc89]. The signature is very clear and this elementary process can be studied in unprecedented detail, as can the self-analyzing polarization of the Λ . The extension to ${}^2_1\text{H}$ in PR 89-045 provides a neutron target and allows one to examine the two-baryon final-state interaction [Me89]. An examination of the hyperon production mechanism in a series of nuclei will be carried out in PR 91-014 [Hy91]. Figure 31.7 shows the projected rates and error bars in PR 91-016 for the production of the lightest bound hypernucleus through ${}^4_2\text{He}(e, e' K^+){}^4_\Lambda\text{H}$ [Ze91]. The bound state is clearly

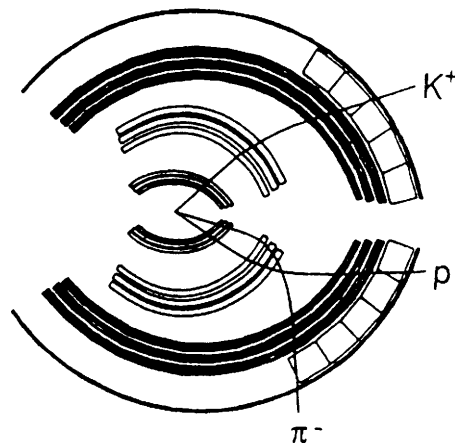


Fig. 31.6. CLAS simulation of ${}^1\text{H}(\gamma, \text{K}^+)\Lambda$ and subsequent decay $\Lambda \rightarrow \text{p} + \pi^-$ from PR 89-004 [Sc89, Wa93].

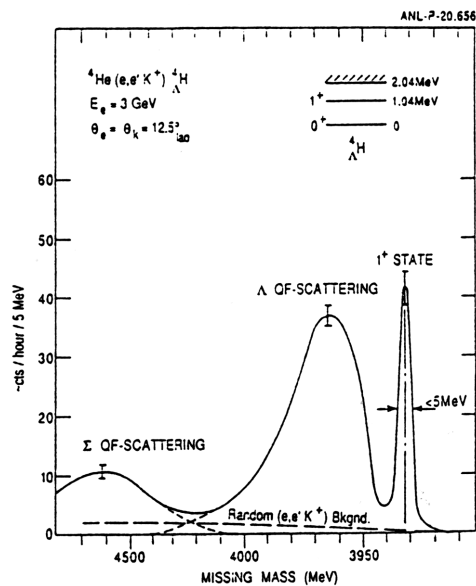


Fig. 31.7. Projected rates and error bars for ${}^4_2\text{He}(e, e' \text{K}^+) {}^4_\Lambda\text{H}$ in PR 91-016 [Ze91, Wa93].

identified in this figure; the projected transition is almost entirely to the spin-flip 1^+ . This experiment forms the prototype for the production of hypernuclei through the $(e, e' \text{K}^+)$ reaction at CEBAF — accessing a whole new dimension of nuclear structure.

Let us return to the subject of parity violation. The nuclear domain consists of (u, d) quarks and their antiquarks. Consider elastic scattering

of polarized electrons from a $(0^+, 0)$ nucleus, for example ${}^{12}_6\text{C}(\vec{e}, e)$. The nuclear quantum numbers serve as a filter, and the standard model states that for such a transition in this sector the weak neutral current and electromagnetic current are strictly proportional

$$\mathcal{J}_\mu^{(0)} \doteq -2 \sin^2 \theta_W J_\mu^\gamma \quad (31.1)$$

The predicted parity-violating asymmetry $\mathcal{A} = (d\sigma_\uparrow - d\sigma_\downarrow)/(d\sigma_\uparrow + d\sigma_\downarrow)$ is then

$$\mathcal{A}_{12\text{C}} = \frac{Gq^2}{\pi\alpha\sqrt{2}} \sin^2 \theta_W \quad (31.2)$$

It is important to note that this result depends only on the existence of isospin symmetry; it holds *to all orders* in the strong interactions (QCD). As we have seen, this quantity has been measured in a tour de force experiment at Bates at $q = 150$ MeV with the result that [So90] ⁶

$$\begin{aligned} \mathcal{A}_{12\text{C}} P_e &= 0.688 \times 10^{-6} && ; \text{theory} \\ &= 0.60 \pm 0.14 \pm 0.02 \times 10^{-6} && ; \text{experiment} \end{aligned} \quad (31.3)$$

This experiment serves as a demonstration of feasibility for the next generation of electron scattering parity-violation experiments.

Now consider the *extended domain* of (u, d, s, c) quarks and their anti-quarks. The standard model then has an additional isoscalar term in the weak neutral current

$$\delta \mathcal{J}_\mu^{(0)} = \frac{i}{2} [\bar{c}\gamma_\mu(1 + \gamma_5)c - \bar{s}\gamma_\mu(1 + \gamma_5)s] \quad (31.4)$$

The asymmetry for elastic scattering of polarized electrons on a $(0^+, 0)$ nucleus such as ${}^4_2\text{He}$ then takes the form

$$\mathcal{A}_{4\text{He}} = \frac{Gq^2}{\pi\alpha\sqrt{2}} \sin^2 \theta_W \left[1 - \frac{\delta F^{(0)}(q^2)}{2 \sin^2 \theta_W F_0^\gamma(q^2)} \right] \quad (31.5)$$

The additional weak neutral current form factor comes from the vector current in Eq.(31.4) — expected to arise predominantly from the much lighter strange quarks. Hence one has a direct measure of the strangeness current in nuclei. The total strangeness of the nucleus must vanish in the strong and electromagnetic sector, and hence $\delta F^{(0)}(0) = 0$; however, just as with the electromagnetic charge in the neutron, there can be a strangeness density, which is determined in this experiment.

Approval exists for the experimental measurements of the asymmetry in ${}^4_2\text{He}(\vec{e}, e)$ in CEBAF PR 91-004 [Be91], and the asymmetry for a similar

⁶ The first error is statistical.

elastic scattering measurement on the nucleon itself ${}^1\text{H}(\vec{\epsilon}, e)$ in CEBAF PR 91-010 [Fi91].⁷ The measurement of the distribution of weak neutral current through $(\vec{\epsilon}, e)$ and $(\vec{\epsilon}, e')$ will be one of the most important results at CEBAF. The beautiful experimental results that now exist on this latter experiment, and their deep implication for the structure of nuclei and nucleons, have already been presented in chapter 27.

In *summary*, let us try to pull all this material together with a statement of the nuclear physics goals of electron scattering studies: first, quite generally, one wants to examine the limits of the traditional, non-relativistic many-body description of the nucleus based on baryons interacting through static potentials fitted to two-body scattering and bound-state data. The nuclear shell model, for example, provides a remarkably successful description of the strongly interacting quantum mechanical nuclear many-body system. Just how far does that description hold, and when does it break down?

The degrees of freedom of the shell model are the nucleons, protons and neutrons. We know from electron scattering that additional sub-nucleonic hadronic degrees of freedom, mesons and isobars, come into play when one examines the nucleus at shorter and shorter distance scales. What is the role of these additional degrees of freedom? The only consistent description we have of a relativistic, interacting, hadronic many-body system is through a relativistic quantum field theory based on a local lagrangian density constructed from the hadronic degrees of freedom. What are the limits of a relativistic, hadronic field theory description of the nuclear system?

At shorter distances still, electron scattering first taught us that quark–gluon degrees of freedom are the relevant ones. At what distance scales are we forced to make the transition from a baryon–meson to a quark–gluon description of the nucleus? The constituent quark model provides a remarkably successful description of the interior structure of the hadrons themselves; however, it is still a model, and just as with the nuclear shell model, one wants to determine where this picture breaks down.

At a more fundamental level, one has a relativistic quantum field theory of the strong interactions, quantum chromodynamics (QCD) based on the strong color interactions of quark and gluons. This is the true relativistic, strongly coupled, nuclear many-body system. As with any theory, the experimental implications of QCD must continually be explored. Electron scattering data will provide the most direct benchmarks against which to test the experimental implications of QCD.

The standard model provides a marvelously successful unified description of the weak and electromagnetic interactions. The experimental im-

⁷ Here the quantum numbers $\frac{1}{2}^+ \frac{1}{2}$ allow other elastic form factors.

plications of the standard model must similarly continue to be explored. Electron scattering provides a tool for examining the weak neutral current distribution in nuclei, which, taken in conjunction with the study of the electromagnetic current distribution effectively doubles the power of electron scattering.

At very short-distance *particle physics* scales, one examines the quark distributions in the nucleon, including those contributing to its spin. At a more basic level, deep-inelastic electron scattering provides an unrivaled tool to examine the short-distance behavior of the relativistic quantum field theory describing the strong interactions, QCD.

Finally, at all levels, we are interested in exploring the *phenomena* manifest by the remarkable, strongly-coupled, quantum-mechanical, nuclear many-body system.